Available online at www.sciencedirect.com
ScienceDirect
Journal of Sound and Vibration 312 (2008) 399–417
JOURNAL OF SOUND AND VIBRATION
www.elsevier.com/locate/jsvi

Analytical and experimental validation of a nondimensional Bingham model for mixed-mode magnetorheological dampers

S.R. Hong[a], N.M. Wereley[a,*], Y.T. Choi[a], S.B. Choi[b]

[a]*Smart Structures Laboratory, Department of Aerospace Engineering, University of Maryland, College Park, MD 20742, USA*
[b]*Smart Structures and Systems Laboratory, Department of Mechanical Engineering, Inha University, Incheon 402-751, Republic of Korea*

Received 27 June 2005; received in revised form 27 June 2007; accepted 9 July 2007
Available online 26 December 2007

Abstract

In this paper an experimental validation of a nondimensional analysis for a mixed-mode magnetorheological (MR) damper is described. Based on the Bingham constitutive equation of an MR fluid, a nondimensional model describing damping capacity of the MR damper is formulated using nondimensional parameters including the Bingham number, nondimensional plug thickness, hydraulic amplification ratio, and equivalent viscous damping coefficient. The effects of the Bingham number and the hydraulic amplification ratio on the nondimensional plug thickness and equivalent viscous damping coefficient are analyzed. A mixed-mode MR damper is designed and fabricated to validate the relationships between nondimensional parameters. The damper is tested under various loading conditions and current (applied magnetic field intensity) levels. The nondimensional parameters and variables are measured experimentally, and the effectiveness of the nondimensional analysis model for mixed-mode MR dampers is demonstrated. In addition, comparisons between mixed and flow mode dampers are undertaken using this nondimensional analysis.

1. Introduction

The field-dependent rheological changes in electrorheological (ER) or magnetorheological (MR) fluids are primarily observed as a significant increase in the yield shear stress of the fluids, which can be continuously controlled by the intensity of applied electric or magnetic field. The field-dependent yield stress of ER or MR fluids can be effectively utilized in semi-active damping control systems. Semi-active devices utilizing ER or MR fluids have the advantages of continuously controllable damping, quiet operation, simple configuration, low power consumption, and high control stability [1,2]. ER or MR dampers have been shown to improve the vibration isolation performances of vehicle suspension systems [3–5], helicopter rotor systems [6], landing gear system [7], and structural systems [8–11].

ER or MR dampers have been designed on the basis of operating modes of the fluids: flow mode (Poiseuille flow) [12–16], shear mode (Couette flow) [14], squeeze (squeeze-flow) mode [17,18], and mixed (Poiseuille and Couette flow) mode [14,19]. Alternatively, a mixed-mode damper utilizes both shear and flow modes in producing damping force.

*Corresponding author. Tel.: +1 301 405 1927; fax: +1 301 314 9001.
E-mail addresses: wereley@umd.edu, wereley@eng.umd.edu (N.M. Wereley).

0022-460X/$ - see front matter © 2007 Elsevier Ltd. All rights reserved.
doi:10.1016/j.jsv.2007.07.087

Shear mode dampers rely on direct shear of ER/MR fluid due to relative motion between two plates where the separation between the two plates is held constant. Flow mode dampers rely on pressurized flow along the axis between two stationary plates, which form the walls of a duct or orifice, to develop damper force. To achieve the same damper force, flow or mixed-mode dampers have the advantage that plates (duct walls) having smaller surface areas than shear mode damper cases can be utilized to achieve the same damper force, so that flow mode dampers can be smaller volume devices. Squeeze mode dampers rely on changes in the plate (duct wall) separation to compress the material and induce flow from between the two plates. Thus, squeeze mode is limited to systems subjected to small magnitude vibrations (low stroke) in order to avoid contact between the two plates. A key advantage of flow or mixed-mode damper operation is that both large force and large stroke can be physically realized.

Various nondimensional models for the analysis of flow or mixed-mode dampers have been studied. For the systematic and comprehensive study of damper characteristics, a nondimensional model that can characterize and predict damper performance would be of great utility. Gavin et al. [20] presented an approximation to the exact solution of a high order nondimensional polynomial to determine the pressure gradient in flow and mixed-mode ER valves [21], and showed that this approximation is useful in analysis of flow or mixed-mode dampers. A flow mode ER damper was tested to validate the proposed nondimensional analysis [12]. Stanway et al. [1,13] studied a nondimensional analysis for a flow mode damper by considering dimensionless numbers of Hedström number, Reynolds number, and a friction factor. In this case, a flow mode ER damper was experimentally analyzed to show the effectiveness of the model. This model has not been extended to mixed-mode damper analysis. Wereley et al. [14,15,22] presented a set of nondimensional groups, consisting of Bingham number, nondimensional plug thickness, and equivalent viscous damping coefficient (dynamic range). The effectiveness of the proposed nondimensional analysis was validated via experiments on flow and mixed-mode ER dampers [14,15], as well as a flow mode MR valve [22]. Hong et al. [16] developed a set of nondimensional groups, consisting of Bingham number, nondimensional geometric parameter, nondimensional damping force, and dynamic range. This nondimensional analysis scheme was effectively applied to design a flow mode ER damper.

As mentioned above, one author of this current study has conducted a nondimensional analysis of a mixed-mode ER damper in previous research [14]. However, some key issues were not considered. First, the Bingham number is defined as the ratio of the dynamic yield stress to the viscous stress [14]. Alternatively, the Bingham number, which can be interpreted as a nondimensional velocity or shear rate, can be defined as a function of either the piston velocity or the average velocity (or shear rate) of the fluid in the valve gap or duct. Hence, the impact of nondimensionalization with respect to piston velocity or average duct velocity must be studied. Second, the piston velocity is related to the average duct velocity by a hydraulic amplification ratio (ratio of cross-sectional piston to duct area). Therefore, the impact of hydraulic amplification on damper force, and its role in interpreting the appropriateness of each Bingham number definition should be examined. The Bingham number and the hydraulic amplification ratio are important factors that determine damper characteristics of mixed-mode dampers.

Therefore, from these perspectives, we will examine further the nondimensional analysis of mixed-mode dampers. To this end, a mixed-mode MR damper is configured and its nondimensional analysis is theoretically constructed by using a set of nondimensional group, consisting of Bingham numbers, hydraulic amplification ratio, nondimensional plug thickness, and equivalent (viscous) damping coefficient. On the basis of the nondimensional analysis, mixed-mode damper characteristics are evaluated and compared with flow mode damper characteristics. To validate the nondimensional analysis of the mixed-mode damper, an MR dashpot damper is designed and fabricated. The relationships of the nondimensional plug thickness and the damping coefficient as a function of both definitions of Bingham number are experimentally validated and the effectiveness of the nondimensional analysis in predicting damper performance is demonstrated.

2. Nondimensional modeling

2.1. Mixed-mode damper

A nondimensional analysis of a mixed-mode dashpot damper featuring MR fluids is studied in this paper and a schematic configuration of the damper is presented in Fig. 1. The MR damper consists of MR fluid reservoir, plunger (or piston), annular gap, electromagnetic coil, flux guide, and housing. The electromagnetic coil supplies a

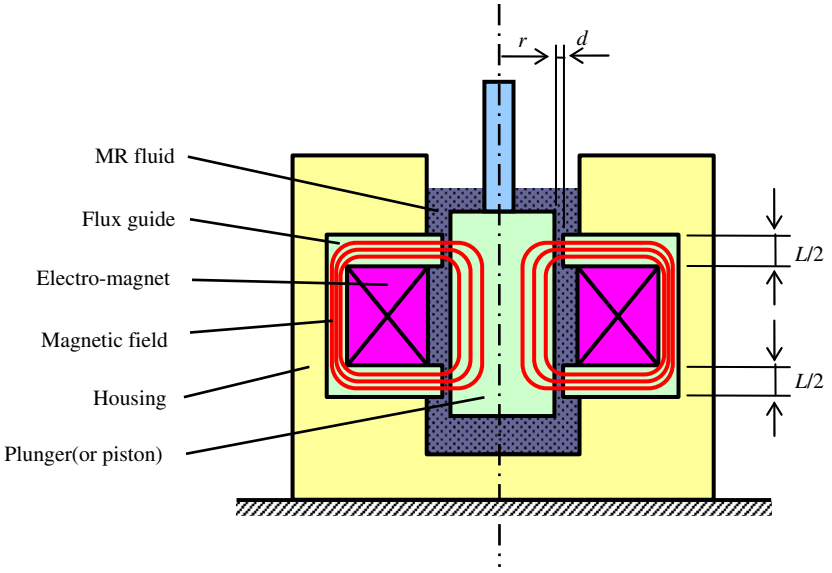

Fig. 1. Schematic configuration of the mixed-mode MR damper.

magnetic field to the MR fluid. The plunger or piston is a loosely fitting piston that travels within the MR fluid reservoir. The MR fluid flows through the annular duct formed by the reservoir wall and the piston outer diameter as the piston moves. The plunger serves to directly shear the fluid between the reservoir wall and the piston wall, as well as to induce pressurized flow through the annular duct. Therefore, the MR damper operates under both shear and flow modes. If no magnetic field is applied, the MR damper only produces a force exerted by the fluid flow resistance associated with the viscosity of the MR fluid. However, if the MR fluid is activated by the magnetic field, the MR damper produces a controllable damping force due to the yield stress of the MR fluid. To simplify the analysis, we will approximate the annular duct as a rectangular duct. If the annular gap is small relative to the annular radius, then the error associated with hydrodynamic analysis is small. However, the errors associated with approximating the radial field in the annular duct as a uniform field in the rectangular duct may have a large impact [23]. We adopt a simple rectangular duct analysis [14] in order to develop physical and analytical insight into the nondimensional behavior of MR dampers.

2.2. Constitutive model

The pressure drop, ΔP, developed via quasi-steady plunger motion can be obtained from force equilibrium in a rectangular duct and is given by

$$\Delta P = -\frac{\mathrm{d}\tau}{\mathrm{d}y} L. \tag{1}$$

Here, τ is the shear stress, y is the coordinate originating from the center of the duct, and L is the active length of the duct. If the ratio of the plunger radius to the gap is large, the governing equation of Bingham plastic flow in a rectangular duct can be applied to approximate mixed-mode flow through an annular duct [14,16,20]. Therefore, Eq. (1) is the starting point for the mixed MR damper analysis in this study. The rheological behavior of MR fluid can be modeled as

$$\begin{aligned} \tau &= \tau_y \operatorname{sgn}\left(\frac{\mathrm{d}u}{\mathrm{d}y}\right) + \mu \frac{\mathrm{d}u}{\mathrm{d}y}, \quad |\tau| > |\tau_y|, \\ \frac{\mathrm{d}u}{\mathrm{d}y} &= 0, \quad |\tau| < |\tau_y|. \end{aligned} \tag{2}$$

Here, τ_y is the field-dependent yield shear stress, u is the fluid velocity, and μ is the plastic viscosity.

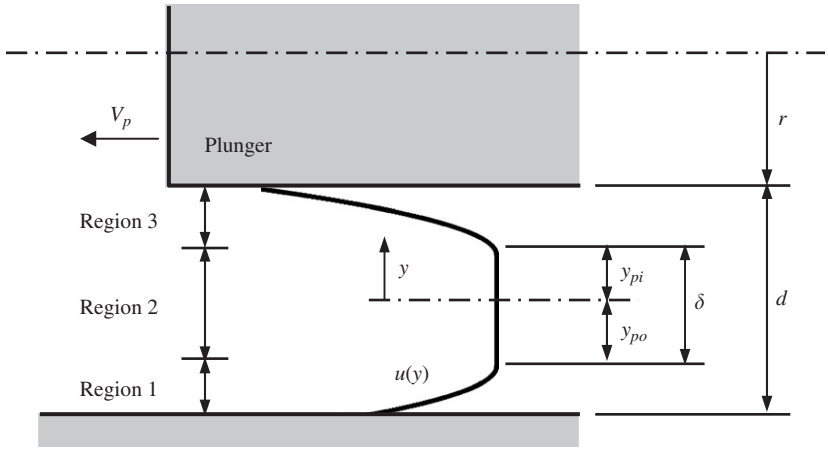

Fig. 2. Schematic diagram of fluid velocity profile in the gap inside the MR damper.

2.3. Velocity profile

A typical velocity profile of MR fluid flow through a rectangular duct is shown in Fig. 2. V_p is the piston velocity, d is the gap, and y_{po} and y_{pi} are locations of the outer and inner edges or boundaries of the plug, respectively. There are three distinct fluid regions exist. Region 1 ($-d/2 \leqslant y \leqslant -y_{po}$) and region 3 ($y_{pi} \leqslant y \leqslant d/2$) are post-yield regions where $|\tau| > \tau_y$, while region 2 ($-y_{po} \leqslant y \leqslant y_{pi}$) is the pre-yield or plug flow region where $|\tau| < \tau_y$.

Since three distinct flow regions exist in the duct, the fluid velocity profiles of each region must be considered separately. The velocity profile of each region can be obtained by direct integration after substituting Eq. (2) into Eq. (1):

$$u_i(y) = -\frac{\Delta P}{2\mu L} y^2 + A_i y + B_i, \quad i = 1, 2, 3. \tag{3}$$

Here, subscript i represents the ith region. A_i and B_i are integration constants to be determined by satisfying velocity boundary and compatibility conditions for each region

$$u_1\left(-\frac{d}{2}\right) = 0, \quad u_1'(-y_{po}) = 0, \quad u_2 = u_3(y_{pi}), \quad u_3\left(\frac{d}{2}\right) = -V_p, \quad u_3'(y_{pi}) = 0. \tag{4}$$

Satisfying these boundary conditions leads to the velocity profile as given below

$$\begin{aligned} u_1(y) &= -\frac{\Delta P}{2\mu L}\left[(y + y_{po})^2 - \left(\frac{d}{2} - y_{po}\right)^2\right], \\ u_2(y) &= \frac{\Delta P}{2\mu L}\left(\frac{d}{2} - y_{pi}\right)^2 - V_p, \\ u_3(y) &= -\frac{\Delta P}{2\mu L}\left[(y - y_{pi})^2 - \left(\frac{d}{2} - y_{pi}\right)^2\right] - V_p. \end{aligned} \tag{5}$$

2.4. Plug thickness

The plug thickness can be determined from Eq. (1) and appropriate shear stress boundary conditions. Integrating Eq. (1) yields the shear stress in the gap as follows:

$$\tau = -\frac{\Delta P}{L} y + C. \tag{6}$$

Here, C is integration constant to be determined using the shear stress boundary conditions

$$\tau(-y_{po}) = \tau_y, \quad \tau(y_{pi}) = -\tau_y, \tag{7}$$

which leads to the system of equations

$$\begin{aligned} \tau_y &= \frac{\Delta P}{L} y_{po} + C, \\ -\tau_y &= -\frac{\Delta P}{L} y_{pi} + C. \end{aligned} \tag{8}$$

Subtraction of the above two equations yields an expression for the plug thickness δ:

$$\delta = y_{po} + y_{pi} = \frac{2L\tau_y}{\Delta P}. \tag{9}$$

Because the plug velocity is constant, the compatibility boundary condition for the constant velocity in the region 2 is given by

$$u_1(y_{po}) = u_3(y_{pi}). \tag{10}$$

Eq. (10) can be expressed by

$$y_{po} - y_{pi} = \frac{2\mu L V_p}{\Delta P(d-\delta)}. \tag{11}$$

The inner and outer plug boundary locations are determined from Eqs. (9) and (11) as follows:

$$\begin{aligned} y_{pi} &= \frac{1}{2}\delta - \frac{\mu L V_p}{\Delta P(d-\delta)}, \\ y_{po} &= \frac{1}{2}\delta + \frac{\mu L V_p}{\Delta P(d-\delta)}. \end{aligned} \tag{12}$$

2.5. Bingham numbers

The equivalent viscous damping can be expressed in terms of the Bingham number and the nondimensional plug thickness $\bar{\delta}(=\delta/d)$ [14]. The Bingham number can be defined as follows [14]:

$$Bi_{V_p} = \frac{\tau_y d}{\mu V_p}. \tag{13}$$

In the above, the piston velocity, or wall velocity, V_p, over the gap, d, accounts for the shear rate of the fluid in the gap. The Bingham number, Bi_{V_p}, is large when the yield shear stress, τ_y, is high, or the plastic viscosity, μ, and the piston velocity, V_p, are low. Therefore, the large Bingham number, Bi_{V_p}, implies that the damper operates at low speed or in a weakly post-yield condition. The Bingham number, Bi_{V_p}, is small, when the piston velocity, V_p, is high, or when the damper is operating in a strongly post-yield condition. The piston velocity, V_p, affects the magnitude of the velocity distribution of the fluid inside the gap. When the piston velocity, V_p, is low, the magnitudes of the velocity or shear rate distributions of the fluid are small. Thus, as the plunger velocity, V_p, decrease, overall velocity or shear rate of the fluid decreases, and the fluid behavior approaches to a weakly post-yield condition.

The velocity of the fluid inside the gap is an actual indicator describing the post-yield condition, and the average duct velocity of the fluid inside the gap, V_d, can be used as the velocity in the Bingham number. Another definition of the Bingham number, considering the average duct velocity, V_d, is given by [15,24]

$$Bi_{V_d} = \frac{\tau_y d}{\mu V_d}. \tag{14}$$

The Bingham number, Bi_{V_d}, incorporates the average velocity of the fluid through the gap, V_d, which is not directly measurable. But the Bingham number, Bi_{V_d}, directly accounts for the fluid behavior inside the gap.

On the other hand, the Bingham number, Bi_{V_p}, incorporates the piston velocity, V_p, which is directly measurable. Therefore, when the damper performance is analyzed with the consideration of the external excitation, or plunger velocity, the Bingham number, Bi_{V_p}, would be preferable. When the damper analysis is focused on the fluid flow inside the gap, which is the direct indication of the Bingham plastic behavior of the fluid, the Bingham number, Bi_{V_d}, is preferred. The average velocity of the fluid, V_d, in the Bingham number, Bi_{V_d}, can be applied to inspecting the flow characteristics of the fluid by using well-known nondimensional variables such as Reynolds number. Although the Bingham numbers, Bi_{V_p} and Bi_{V_d}, incorporate different velocity terms, they provide common physical intuition. Both Bingham numbers being large implies that the dampers operate at low speed or in a weakly post-yield condition. The Bingham numbers are both zero when the dynamic yield shear stress is zero, as is nearly the case in the absence of field. In this work, nondimensional analyses considering both definitions of the Bingham number will be treated and their influences on the damping capacity of the damper will be analyzed.

2.6. Hydraulic amplification ratio

The velocities, V_p and V_d, are related by

$$V_d = \bar{A} V_p = \frac{A_p}{A_d} V_p. \tag{15}$$

Here, $\bar{A}$ is the hydraulic amplification ratio or area ratio defined by the ratio of the piston head area, A_p, to the cross-sectional area of the gap, $A_d\,(=bd)$. Also, b is the width of the duct (or the average circumference of the annular duct). From Eqs. (13)–(15), the relationship between the Bingham numbers is given by

$$Bi_{V_p} = \bar{A} Bi_{V_d}. \tag{16}$$

Note that these Bingham numbers yield different values at the same operating condition or damper shaft speed.

2.7. Nondimensional velocity profile

A convenient nondimensional form of velocity profile Eq. (5) can be obtained by introducing the following:

$$\bar{y} = \frac{y}{d}, \quad \bar{u} = \left[\frac{2\mu L}{\Delta P}\left(\frac{2}{d}\right)^2\right] u. \tag{17}$$

Here, $\bar{y}$ is nondimensional gap coordinate and $\bar{u}$ is nondimensional velocity profile. From Eqs. (5), (13) and (17), the nondimensional velocity profiles of each region are expressed by

$$\begin{aligned}
\bar{u}_1(y) &= -\left(2\bar{y} + \bar{\delta} + \frac{\bar{\delta}}{1-\bar{\delta}}\frac{1}{Bi_{V_p}}\right)^2 + \left(1 - \bar{\delta} - \frac{\bar{\delta}}{1-\bar{\delta}}\frac{1}{Bi_{V_p}}\right)^2,\\
\bar{u}_2(y) &= \left(1 - \bar{\delta} + \frac{\bar{\delta}}{1-\bar{\delta}}\frac{1}{Bi_{V_p}}\right)^2 - 4\bar{\delta}\frac{1}{Bi_{V_p}},\\
\bar{u}_3(y) &= -\left(2\bar{y} - \bar{\delta} + \frac{\bar{\delta}}{1-\bar{\delta}}\frac{1}{Bi_{V_p}}\right)^2 + \left(1 - \bar{\delta} + \frac{\bar{\delta}}{1-\bar{\delta}}\frac{1}{Bi_{V_p}}\right)^2 - 4\bar{\delta}\frac{1}{Bi_{V_p}}.
\end{aligned} \tag{18}$$

Given the nondimensional plug thickness, $\bar{\delta}$, and the Bingham number, Bi_{V_p}, the nondimensional velocity profile, $\bar{u}$, can be achievable. On the other hand, the nondimensional velocity profiles of flow mode damper are given by [25–27]

$$\begin{aligned}
\bar{u}_1(y) &= -(2\bar{y} + \bar{\delta})^2 + (1-\bar{\delta})^2,\\
\bar{u}_2(y) &= (1-\bar{\delta})^2,\\
\bar{u}_3(y) &= -(2\bar{y} - \bar{\delta})^2 + (1-\bar{\delta})^2.
\end{aligned} \tag{19}$$

2.8. Equivalent damping coefficient

The yield shear stress from Eq. (9) is expressed as

$$\tau_y = \frac{\bar{\delta} d\,\Delta P}{2L} = \frac{\bar{\delta} dF}{2LA_p}. \tag{20}$$

Here, $F(=A_p\Delta P)$ is the damper force exerted on the mixed-mode damper. Using Eqs. (13) and (20), the equivalent viscous damping, C_{eq}, is obtained by

$$C_{\mathrm{eq}} = \frac{F}{V_p} = \frac{2\mu L A_p}{d^2}\frac{Bi_{V_p}}{\bar{\delta}}. \tag{21}$$

The relationship between nondimensional variables, that is the Bingham number, Bi_{V_p}, and nondimensional plug thickness, $\bar{\delta}$, can be found by equating the total volume flux through the duct, Q_d, to the volume flux displaced by the piston, Q_p. The volume flux through the duct, Q_d, is

$$Q_d = Q_1 + Q_2 + Q_3, \tag{22}$$

where

$$\begin{aligned}
Q_1 &= b\int_{-d/2}^{-y_{po}} u_1(y)\,\mathrm{d}y = \frac{1}{24}\frac{b\,\Delta P d^3}{\mu L}\left[1-\bar{\delta}-\frac{\bar{\delta}}{(1-\bar{\delta})Bi_{V_p}}\right]^3,\\
Q_2 &= b\int_{-y_{po}}^{y_{pi}} u_2(y)\,\mathrm{d}y = \frac{1}{8}\frac{b\,\Delta P d^3}{\mu L}\left[1-\bar{\delta}+\frac{\bar{\delta}}{(1-\bar{\delta})Bi_{V_p}}\right]^2\bar{\delta} - \frac{1}{2}\frac{b\,\Delta P d^3}{\mu L}\frac{\bar{\delta}^2}{Bi_{V_p}},\\
Q_3 &= b\int_{y_{pi}}^{d/2} u_3(y)\,\mathrm{d}y = \frac{1}{24}\frac{b\,\Delta P d^3}{\mu L}\left[1-\bar{\delta}+\frac{\bar{\delta}}{(1-\bar{\delta})Bi_{V_p}}\right]^2\bar{\delta} - \frac{1}{4}\frac{b\,\Delta P d^3}{\mu L}\left[1+\bar{\delta}+\frac{\bar{\delta}}{(1-\bar{\delta})Bi_{V_p}}\right]\bar{\delta}.
\end{aligned} \tag{23}$$

The total volume flux, Q_d, equals the volume flux displaced by the piston head, Q_p, so that

$$Q_d = Q_p = A_p V_p = \frac{1}{2}\frac{\Delta P d^2 A_p}{\mu L}\frac{\bar{\delta}}{Bi_{V_p}}. \tag{24}$$

From Eqs. (22)–(24), the relationship between the nondimensional variables is

$$6\bar{\delta}\left(\frac{1}{2}+\bar{A}\right)\frac{1+\sqrt{1-\bar{\delta}/6(1+\bar{\delta}/2)(\bar{A}+1/2)^{-2}}}{2(1-\bar{\delta})^2(1+\bar{\delta}/2)} = Bi_{V_p}. \tag{25}$$

Given the hydraulic amplification ratio, $\bar{A}$, and the Bingham number, Bi_{V_p}, the nondimensional plug thickness, $\bar{\delta}$, can be determined using a root finding algorithm. Eq. (25) has only one physically realizable solution that satisfies $0<\bar{\delta}<1$.

Damping can be expressed by substituting the Bingham number, Bi_{V_p}, of Eq. (25) into Eq. (21) and rearranging Eq. (21) such that

$$C_{\mathrm{eq}} = \frac{12\mu A_p L}{d^2}\left(\frac{1}{2}+\bar{A}\right)\frac{1+\sqrt{1-\bar{\delta}/6(1+\bar{\delta}/2)(\bar{A}+1/2)^{-2}}}{2(1-\bar{\delta})^2(1+\bar{\delta}/2)}. \tag{26}$$

From Eq. (26), the damping coefficient defined by the ratio of the equivalent viscous damping, C_{eq}, to the Newtonian viscous damping, C_0, is given by

$$\frac{C_{\mathrm{eq}}}{C_0} = \frac{1+\sqrt{1-\bar{\delta}/6(1+\bar{\delta}/2)(\bar{A}+1/2)^{-2}}}{2(1-\bar{\delta})^2(1+\bar{\delta}/2)}, \tag{27}$$

where

$$C_0 = \frac{12\mu A^2 L}{d^2}\left(\frac{1}{2} + \bar{A}\right). \tag{28}$$

Note that Eq. (27) is the principal nondimensional representation of the damping capacity of the mixed-mode MR damper.

Alternatively, an analogous set of nondimensional relationships can be obtained using the Bingham number, Bi_{V_p}. By substituting Bi_{V_p} from Eq. (16) into Eq. (25), the relationship between the nondimensional variables is

$$6\bar{\delta}\left(1 + \frac{1}{2\bar{A}}\right)\frac{1 + \sqrt{1 - \bar{\delta}/6(1 + \bar{\delta}/2)(\bar{A} + 1/2)^{-2}}}{2(1 - \bar{\delta})^2(1 + \bar{\delta}/2)} = Bi_{V_d}. \tag{29}$$

The equivalent damping equations accounting for the Bingham number, Bi_{V_d}, have the same forms as Eqs. (26)–(28) for the Bingham number, Bi_{V_p}. As can be seen from Eqs. (25) and (29), a given nondimensional plug thickness corresponds to two different values of the Bingham numbers, Bi_{V_p} and Bi_{V_d}.

On the other hand, the damping coefficient for the flow mode damper is [14,15]

$$\frac{C_{\mathrm{eq}}}{C_0} = \frac{1}{(1 - \bar{\delta})^2(1 + \bar{\delta}/2)}. \tag{30}$$

The relationships between the nondimensional parameters in flow mode damper are [14,15]

$$\begin{aligned} 6\bar{A}\frac{\bar{\delta}}{(1 - \bar{\delta})^2(1 + \bar{\delta}/2)} &= Bi_{V_p}, \\ 6\frac{\bar{\delta}}{(1 - \bar{\delta})^2(1 + \bar{\delta}/2)} &= Bi_{V_d}. \end{aligned} \tag{31}$$

The above nondimensional equations will be used to compare the characteristics between flow and mixed-mode dampers. It is noted that the hydraulic amplification ratio does not appear in Eq. (30). Furthermore, the nondimensional plug thickness equation with Bingham number, Bi_{V_d}, also does not contain the hydraulic amplification ratio, $\bar{A}$. These imply that the Bingham number using duct velocity, Bi_{V_d}, provides a more concise nondimensional analysis for flow mode dampers than does the Bingham number, Bi_{V_p}, based on the piston velocity.

3. Nondimensional analysis

3.1. Nondimensional velocity profile

From Eqs. (18) and (25), the nondimensional velocity profile is a function of the nondimensional plug thickness, $\bar{\delta}$, and hydraulic amplification ratio, $\bar{A}$. For the case of $\bar{A} = 3$, the nondimensional fluid velocity profile is presented in Fig. 3(a). When the plug thickness, $\bar{\delta}$, is zero, the nondimensional velocity profile is parabolic, which is indicative of Newtonian shear flow. The velocity at the plunger side is not zero because the plunger is moving with nondimensional velocity of $-4\bar{\delta}/Bi_{V_p}$. As the plug thickness, $\bar{\delta}$, increases from zero, the plug or pre-yield region extends and the plug velocity decreases. This implies that the flow resistance in the gap or duct increases.

The nondimensional velocity profile for $\bar{A} = 27$ is presented in Fig. 3(b). Comparing the profile for $\bar{A} = 27$ to that for $\bar{A} = 3$, it is clearly seen that the plunger side plunger velocity is close to zero. Therefore, when the hydraulic amplification ratio, $\bar{A}$, is large, the fluid flow behavior of the mixed-mode damper approaches that of the flow mode damper case.

The nondimensional velocity profiles for the flow mode damper are also presented in Fig. 3 and compared with the mixed-mode damper cases. We observe the large difference in the velocity profiles

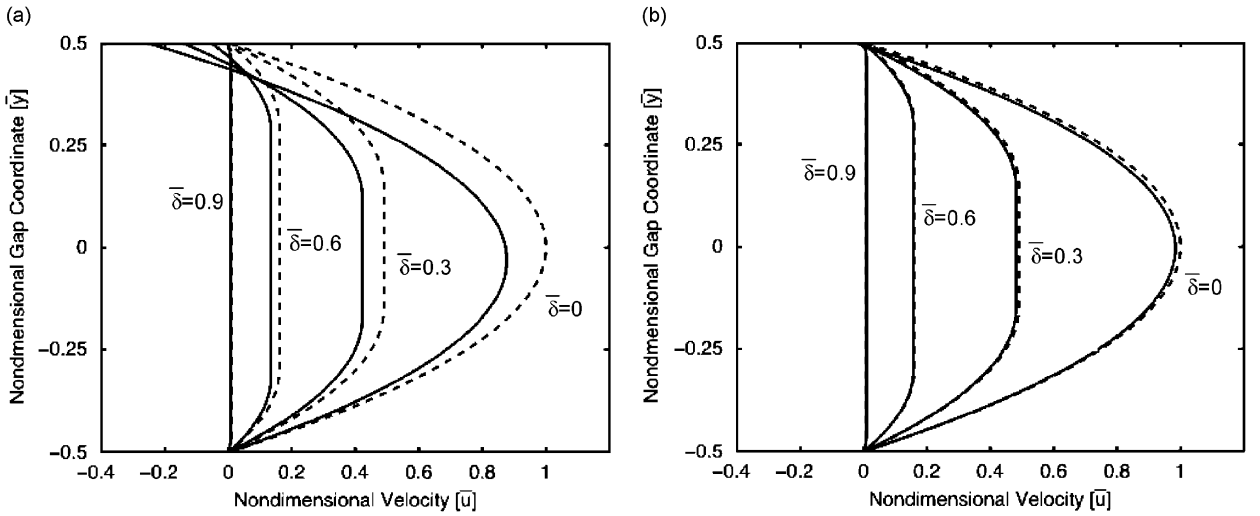

Fig. 3. Nondimensional velocity profiles of the fluid in the gap: (a) $\bar{u}$ versus $\bar{y}$ at various $\bar{\delta}$ at $\bar{A}=3$ and (b) $\bar{u}$ versus $\bar{y}$ at various $\bar{\delta}$ at $\bar{A}=27$: (——) mixed mode and (- - - - -) flow mode.

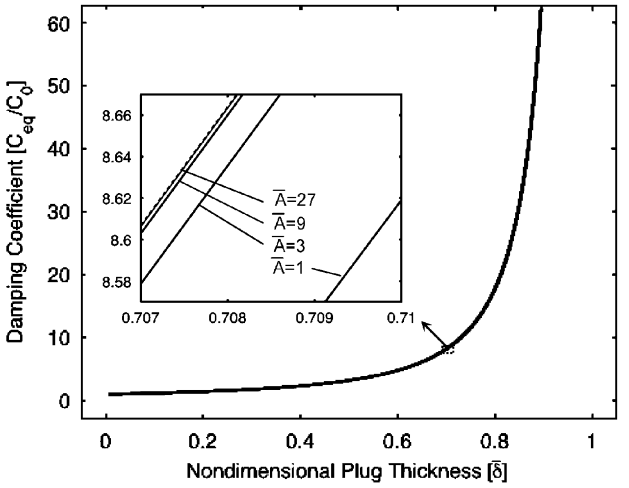

Fig. 4. Damping coefficient versus nondimensional plug thickness: (——) mixed mode and (- - - - -) flow mode.

when $\bar{A}=3$. In contrast, the velocity profiles when $\bar{A}=27$ are similar, which implies that the dynamic characteristics of flow and mixed-mode dampers are similar when the hydraulic amplification ratio, $\bar{A}$, is large.

3.2. Damping coefficient versus nondimensional plug thickness

The damping coefficient, C_{eq}/C_0, is represented as a function of the nondimensional plug thickness, $\bar{\delta}$, and the hydraulic amplification ratio, $\bar{A}$, in Fig. 4. As the nondimensional plug thickness, $\bar{\delta}$, increases, the damping coefficient, C_{eq}/C_0, also increases. On the other hand, the damping coefficient, C_{eq}/C_0, versus the nondimensional plug thickness, $\bar{\delta}$, is not much affected by the hydraulic amplification ratio, $\bar{A}$. Therefore, the damping coefficient, C_{eq}/C_0, is dominantly determined by the plug thickness, $\bar{\delta}$. It is noted that as the

hydraulic amplification ratio, $\bar{A}$, increases, the damping coefficient, C_{eq}/C_0, of the mixed-mode damper approaches to the flow mode damper case.

3.3. Nondimensional plug thickness versus Bingham numbers

The relationship of the nondimensional plug thickness, $\bar{\delta}$, and the Bingham number, Bi_{V_p}, with the influence of the hydraulic amplification ratio, $\bar{A}$, is presented in Fig. 5(a). As the Bingham number, Bi_{V_p}, increases, the nondimensional plug thickness $\bar{\delta}$ increases. By increasing the Bingham number, Bi_{V_p}, a high nondimensional plug thickness, $\bar{\delta}$, can be obtained and approaches one. When the nondimensional plug thickness, $\bar{\delta}$, is one, the plug is fully developed inside the gap, and the flow does not occur. As the dynamic yield shear stress, τ_y, increases or the piston velocity, V_p, decreases, the plug becomes larger. When the yield shear stress, τ_y, is reduced to zero or the piston velocity, V_p, approaches infinity, the Bingham number, Bi_{V_p}, and the nondimensional plug thickness $\bar{\delta}$ approach zero. This is the case of Newtonian flow.

By increasing the hydraulic amplification ratio, $\bar{A}$, the nondimensional plug thickness, $\bar{\delta}$, decreased. For a given Bingham number, Bi_{V_p}, or piston velocity, V_p, the increase of the hydraulic amplification ratio, $\bar{A}$, implies an increase in piston area, A_p, and average duct velocity, V_d. Thus, this results in an increase in shear rate across the gap, and a decrease in the nondimensional plug thickness, $\bar{\delta}$.

On the other hand, the gap, d, affects both the Bingham number, Bi_{V_p}, and the hydraulic amplification ratio, $\bar{A}$. Enlarging the gap, d, increases the Bingham number, Bi_{V_p}, and reduces the hydraulic amplification ratio, $\bar{A}$. Therefore, a higher nondimensional plug thickness, $\bar{\delta}$, can be obtained by increasing the gap.

Fig. 5(b) presents the relationship of the nondimensional plug thickness, $\bar{\delta}$, and the Bingham number, Bi_{V_d}, with the influence of the hydraulic amplification ratio, $\bar{A}$. The basic role of the Bingham number, Bi_{V_d}, is the same as the Bingham number Bi_{V_p}. As the Bingham number, Bi_{V_d}, increases, the nondimensional plug thickness, $\bar{\delta}$, increases.

As the hydraulic amplification ratio, $\bar{A}$, increases for a given Bingham number, Bi_{V_d}, the nondimensional plug thickness, $\bar{\delta}$, also increases. For a given Bingham number, Bi_{V_d}, with an average duct velocity, V_d, a large hydraulic amplification ratio, $\bar{A}$, implies that the piston area, A_p, is large, or the piston velocity (or wall velocity), V_p, is low to satisfy flow continuity, so that the magnitude of fluid velocity distribution across the duct decreases. Therefore, the plug can be easily developed when the hydraulic amplification ratio, $\bar{A}$, is high. Furthermore, when the hydraulic amplification ratio, $\bar{A}$, tends to infinity, a piston velocity, V_p, approaches

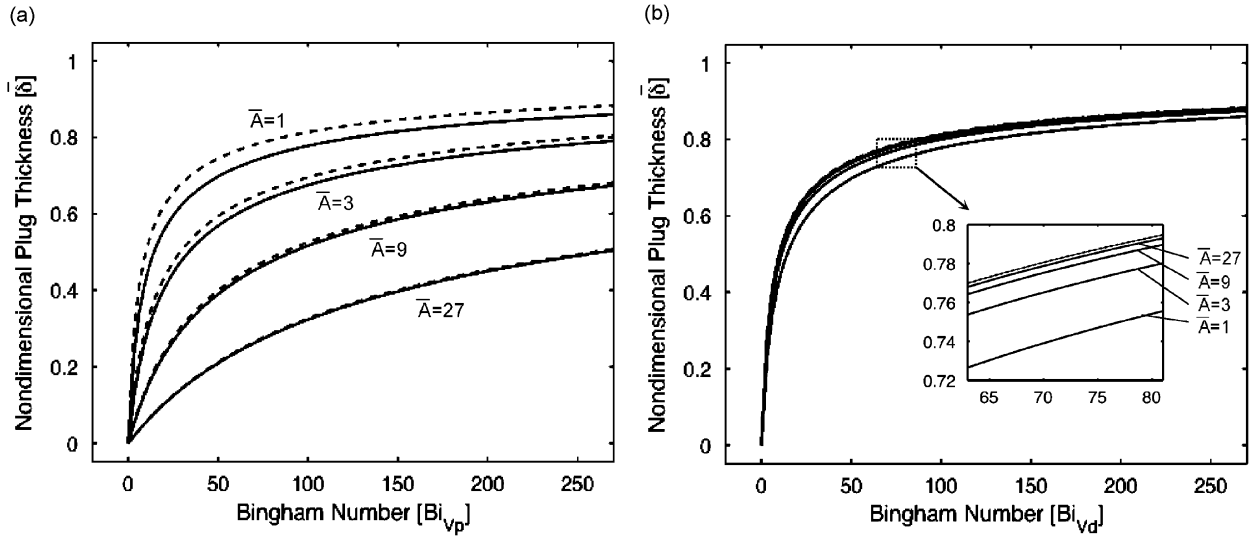

Fig. 5. Nondimensional plug thickness versus Bingham numbers: (a) $\bar{\delta}$ versus Bi_{V_p} at various $\bar{A}$ and (b) $\bar{\delta}$ versus Bi_{V_d} at various $\bar{A}$: (——) mixed mode and (- - - - -) flow mode.

to zero. This implies that the mixed-mode damper characteristics reduce to those of the flow mode damper case.

Although the tendencies of the nondimensional plug thickness, $\bar{\delta}$, with respect to the variation of the hydraulic amplification ratio, $\bar{A}$, depend on the Bingham numbers, both nondimensional relations of Figs. 5(a) and (b) are physically reasonable and give an insight into the analysis and design of the damper. The Bingham number, Bi_{V_p}, can provide useful insights on the damper design schemes by directly considering the external loading condition such as piston velocity. If the Bingham number, Bi_{V_p}, is given from fluid properties, gap, and piston velocity, the appropriate hydraulic amplification ratio, $\bar{A}$, can be easily chosen to meet a desired nondimensional plug thickness, $\bar{\delta}$. On the other hand, the damper force generated in the duct inside the damper is directly affected by the flow rate of the fluid through the duct. Therefore, the Bingham number, Bi_{V_d}, represents directly the operating condition of the fluid inside the duct, and can be an absolute indicator of the damper characteristics.

The relationships between the nondimensional parameters of the flow mode damper are presented in Fig. 5 for comparison with mixed-mode damper results. As the hydraulic amplification, $\bar{A}$, increases, the nondimensional plug thicknesses, $\bar{\delta}$, of flow and mixed-mode dampers become closer for a given Bingham numbers. This implies when the hydraulic amplification, $\bar{A}$, is large, the relationships of nondimensional parameters of flow model damper, which has a simple form, can be used successfully to analyze the mixed-mode damper. On the other hand, when the hydraulic amplification, $\bar{A}$, is small, the mixed-mode damper analysis should be used to analyze a mixed-mode damper.

3.4. Damping coefficient versus Bingham numbers

The relationship between the damping coefficient, C_{eq}/C_0, and the Bingham numbers, Bi_{V_p} and Bi_{V_d}, with the influence of the hydraulic amplification ratio, $\bar{A}$, is presented in Figs. 6(a) and (b). As the Bingham numbers, Bi_{V_p} and Bi_{V_d}, increase, and the damping coefficients, C_{eq}/C_0, also increase. When the Bingham numbers tend to zero, as in the case of strongly post-yield flows, the plug thickness also tends to zero, and the damping coefficient, C_{eq}/C_0, approaches one. Thus, the equivalent viscous damping tends to the Newtonian damping as Bingham number grows small.

For given Bingham numbers, Bi_{V_p} and Bi_{V_d}, the damping coefficient, C_{eq}/C_0, with respect to the hydraulic amplification ratio, $\bar{A}$, show similar trends but vary quantitatively. This can be expected from the nondimensional plug thickness, $\bar{\delta}$, with respect to the hydraulic amplification ratio, $\bar{A}$, as presented in Fig. 5.

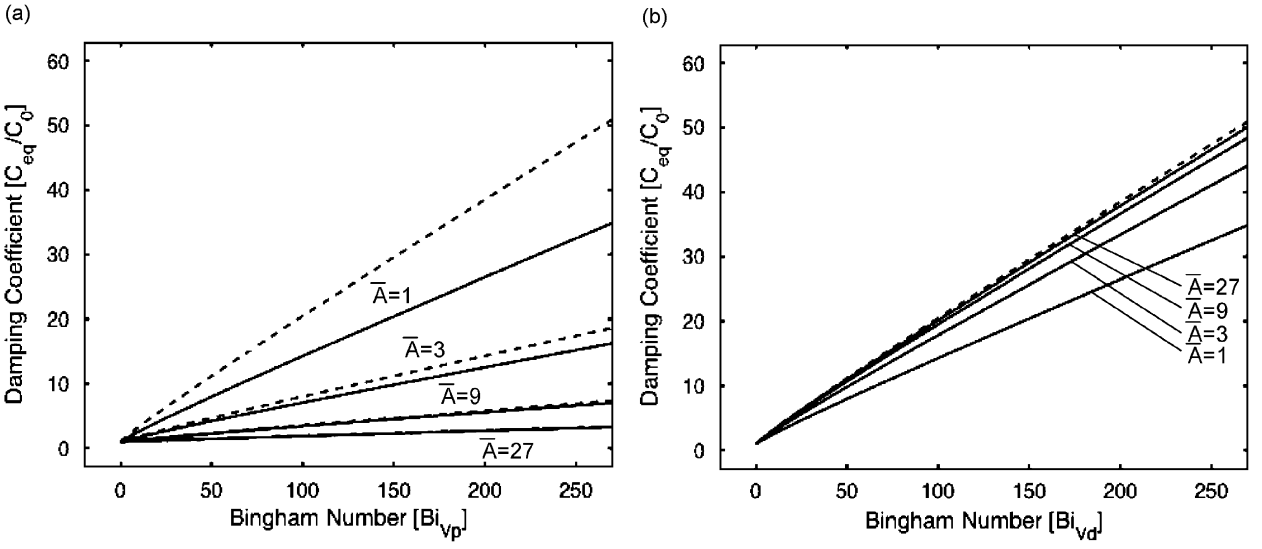

Fig. 6. Damping coefficient versus Bingham numbers: (a) C_{eq}/C_0 versus Bi_{V_p} at various $\bar{A}$ and (b) C_{eq}/C_0 versus Bi_{V_d} at various $\bar{A}$: (——) mixed mode and (- - - - -) flow mode.

The damping coefficients of the flow mode damper are also presented in Fig. 6. When the value of the hydraulic amplification, $\bar{A}$, is small, the difference between flow and mixed-mode damping coefficients are significant. Thus, when we analyze the damping of a mixed-mode damper which has a small value of hydraulic amplification, $\bar{A}$, the mixed-mode damper model must be used.

4. Experimental validation

4.1. Mixed-mode damper design

For the experimental validation of the mixed-mode damper models, an MR dashpot damper was manufactured and tested. If the hydraulic amplification ratio is large, or $\bar{A} \gg 1$, the characteristics of the flow and mixed-mode dampers are indistinguishable. But if the hydraulic amplification ratio is small, or $\bar{A} > 1$, the mixed-mode damper must be analyzed using the mixed-mode damper model. Therefore, the MR dashpot damper with small hydraulic amplification ratio, $\bar{A} = 2.71$ was designed in this study. The geometry of the MR dashpot damper was as follows: the active length of the duct, $L = 10$ mm, the piston head radius, $r = 8.5$ mm, and the gap, $d = 1.5$ mm. MR fluid filled in the damper was Lord Corporation MRF-132LD.

4.2. Experimental setup and testing

In order to measure the damper force, the damper was placed between a load cell and an electromagnetic exciter. An accelerometer measured the acceleration of the exciter table, and the signal generated from this accelerometer was fed back to the exciter controller for the regulation of the excitation velocity. The excitation velocity was obtained by integrating the acceleration signal. When the shaker table moved in response to a command signal from the exciter controller, a damping force was measured using the load cell. To generate magnetic field across the gap of the annular duct in the damper, a current supply was used. The current I applied to the electromagnetic coil ranged from 0.0 to 1.2 A in increments of 0.4 A, or the magnetic field, applied across the annular gap, ranged from 0.0 to 20.7 kA/m in increments of 6.9 kA/m. The excitation velocities were sinusoidal with amplitudes, $V_a = 0.03$, 0.05, and 0.07 m/s, and frequencies, $f = 20$, 30, 40 Hz, respectively. The total number of damper test conditions was $32 (= 4 \times 3 \times 3)$.

4.3. Measured force

Figs. 7(a) and (b) show the force vs. velocity and force vs. displacement cycle data with respect to the applied current. The excitation velocity amplitude and frequency were set to 0.07 m/s and 20 Hz, respectively. From the force vs. velocity plot of Fig. 7(a), it is observed that the Bingham plastic behavior is manifested which consists of the viscous damping force and field-dependent yield force. As the current increases, the yield force also increases. Although loops arise due to fluid inertia effects in the high velocity region and compliance effect in the low velocity region, the overall or average damper force behavior reflects the Bingham plastic model. As the current increases the area within the force vs. displacement hysteresis cycle increases. The energy dissipated by a damper over one vibration cycle is a measure of its damping capacity, and is given by the area enclosed with the force vs. displacement cycle. As can be seen from Fig. 7(b), when the current is high, the area within the force vs. displacement cycle is large, and this indicates the increase in damping or energy dissipation by the damper.

Fig. 8(a) shows the force vs. velocity cycles with respect to excitation velocity frequencies of 20, 30, and 40 Hz. The velocity amplitude and current were set to 0.05 m/s and 1.2 A, respectively. The (high speed) inertia and (low speed) hysteresis loops have a dependency on the excitation frequency, but the behavior of the damper yield force and post-yield damping is representative of the Bingham plastic model. The yield force and post-yield damping were not very sensitive to changes in excitation frequency. Fig. 8(b) shows the force vs. velocity cycles with respect to the excitation velocity amplitudes of 0.03, 0.05, and 0.07 m/s. The excitation frequency and current were set to 30 Hz and 1.2 A, respectively. As the excitation velocity amplitude increased, the post-yield damping decreased. The variation of the post-yield damping is dominated by the shear thinning effect of the employed MR fluid and will be accounted for in the validation of the nondimensional model.

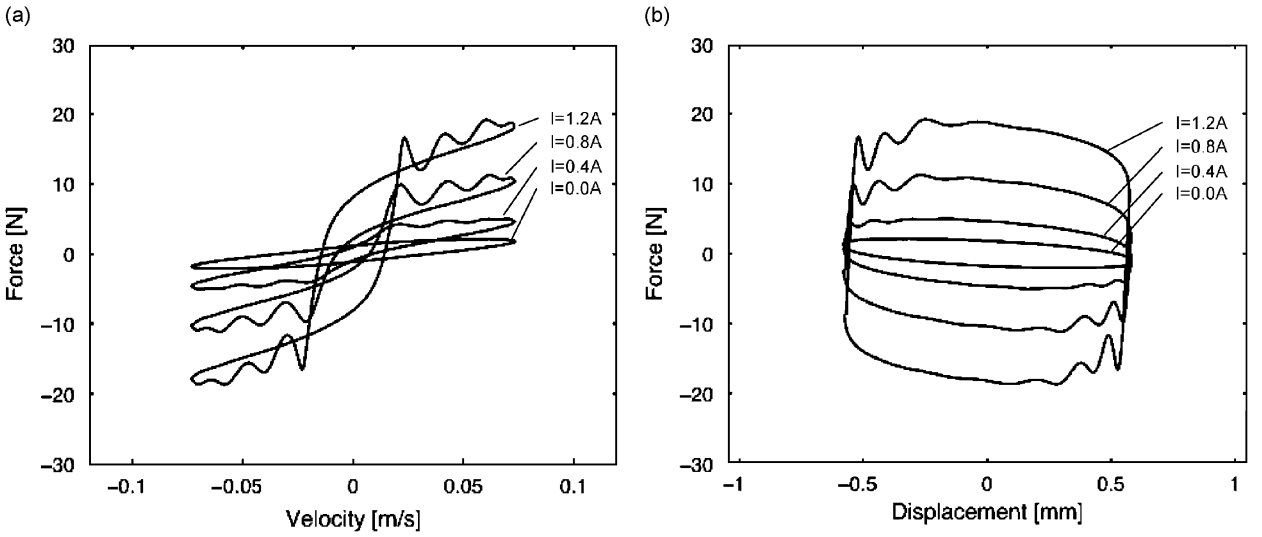

Fig. 7. Measured forces for different field strengths ($V_a = 0.07$ m/s and $f = 20$ Hz): (a) force versus velocity and (b) force versus displacement.

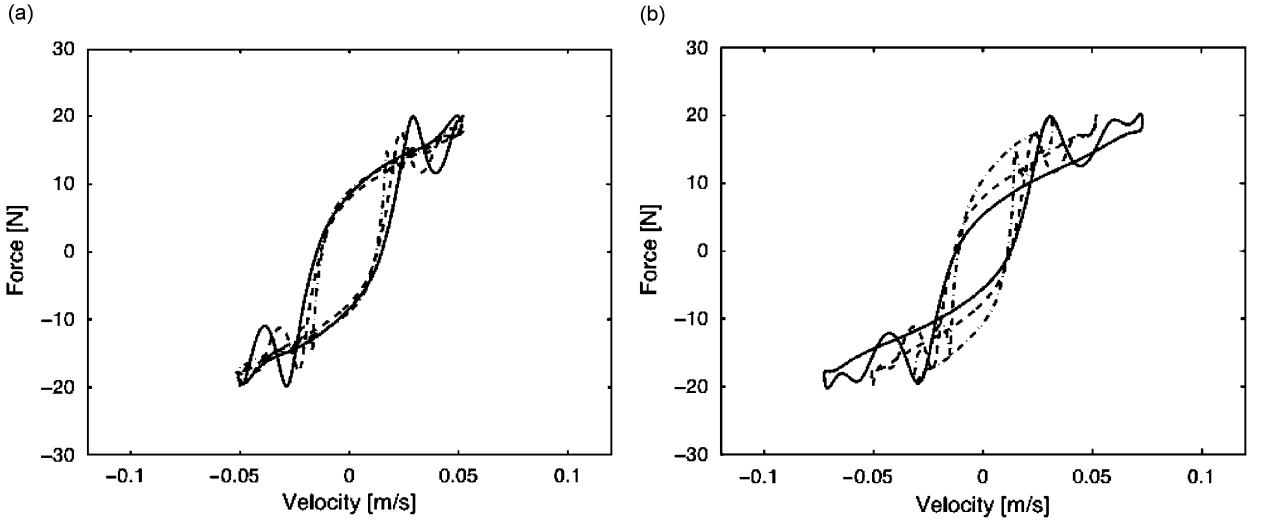

Fig. 8. Measured forces for different excitation conditions ($I = 1.2$ A): (a) excitation frequency variation ($V_a = 0.05$ m/s), (– · –) $f = 20$ Hz, (– – –) 30 Hz, and (——) 40 Hz and (b) excitation amplitude variation ($f = 30$ Hz), $V_a =$ (– · –) 0.03 m/s, (– – –) 0.05 m/s, and (——) 0.07 m/s.

4.4. Equivalent damping

The energy dissipated by an MR damper over one vibration cycle, U, is given by the integral

$$U = \oint F \, \mathrm{d}X_p = \int_0^{2\pi/\omega} F V_p \, \mathrm{d}t. \tag{32}$$

Here X_p is the piston displacement and ω is the radial frequency of the excitation. An equivalent viscous damping, C_{eq}, can be determined by equating the dissipated energy by the MR damper to that of an equivalent

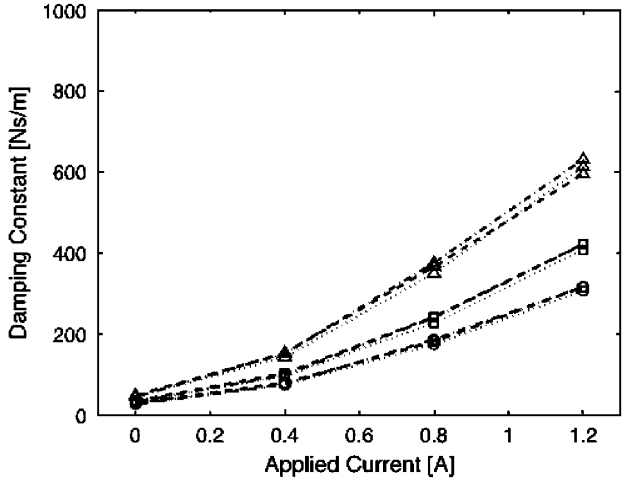

Fig. 9. Experimental damping constant versus applied current: (·····△·····) $V_a = 0.03$ m/s, $f = 20$ Hz; (-·-△-·-) $V_a = 0.03$ m/s, $f = 30$ Hz; (- -△- -) $V_a = 0.03$ m/s, $f = 40$ Hz; (·····□·····) $V_a = 0.05$ m/s, $f = 20$ Hz; (-·-□-·-) $V_a = 0.05$ m/s, $f = 30$ Hz; (- -□- -) $V_a = 0.05$ m/s, $f = 40$ Hz; (·····○·····) $V_a = 0.07$ m/s, $f = 20$ Hz; (-·-○-·-) $V_a = 0.07$ m/s, $f = 30$ Hz; and (- -○- -) $V_a = 0.07$ m/s, $f = 40$ Hz.

viscous damper as follows:

$$C_{\text{eq}} = \frac{U}{\pi\omega X_a^2}, \tag{33}$$

where X_a is the amplitude of the piston displacement, X_p.

Fig. 9 shows the equivalent viscous damping, C_{eq}, calculated by using measured data and Eqs. (32) and (33). It is clearly observed that the equivalent viscous damping is highest when the applied current is high and the excitation velocity amplitude is low. The excitation frequency has minimal effect on the equivalent damping. This implies the fluid inertia effects can be neglected in the damping analysis in this test frequency range. Thus, the equivalent damping obtained by damper test reflects typical Bingham plastic behavior that characterized by the field intensity and fluid velocity magnitude.

4.5. Bingham numbers

For the damper analysis using the nondimensional model, the Bingham numbers, Bi_{V_p} and Bi_{V_d}, of Eqs. (13) and (14) should be obtained as a first step. For given Bingham numbers, Bi_{V_p} and Bi_{V_d}, and hydraulic amplification ratio, $\bar{A}$, the nondimensional plug thickness, $\bar{\delta}$, can be determined by numerically solving for the roots of Eqs. (25) and (29). And then, the equivalent viscous damping coefficient can be analytically obtained by using Eqs. (27) and (28). The parameters for the evaluation of the Bingham numbers related as follows. Because the damper was tested under dynamic loading, the piston velocity, V_p, for the Bingham number, Bi_{V_p}, was given by the rms value of the excitation velocity. The average velocity of the fluid, V_d, for the Bingham number, Bi_{V_d}, was also obtained by considering the amplification ratio, $\bar{A}(= 2.71)$, and the rms value of the excitation velocity. Therefore, the rms velocities for the calculation of the Bingham numbers are given by

$$V_{p,\text{rms}} = \left(\frac{1}{2\pi/\omega}\int_0^{2\pi/\omega} V_p^2\,\mathrm{d}t\right)^{1/2} = \frac{V_a}{\sqrt{2}},$$
$$V_{d,\text{rms}} = \frac{\bar{A}V_a}{\sqrt{2}}. \tag{34}$$

In the above, V_a is the amplitude of the piston velocity, V_p.

4.6. MR fluid properties

The fluid properties, the viscosity and the yield shear stress, are also required for the determination of the Bingham numbers. Fig. 10(a) shows the fluid viscosity found by using Eq. (25) and zero field damping of Fig. 9 at each average velocity of the fluid in the gap, V_d. When the average velocity of the fluid is high, the viscosity of the fluid becomes low. This implies the employed fluid in this study exhibits shear thinning behavior. Fig. 10(b) shows the yield shear stress of the fluid chosen by maximizing the correlation between the experimental and analytical damping coefficients.

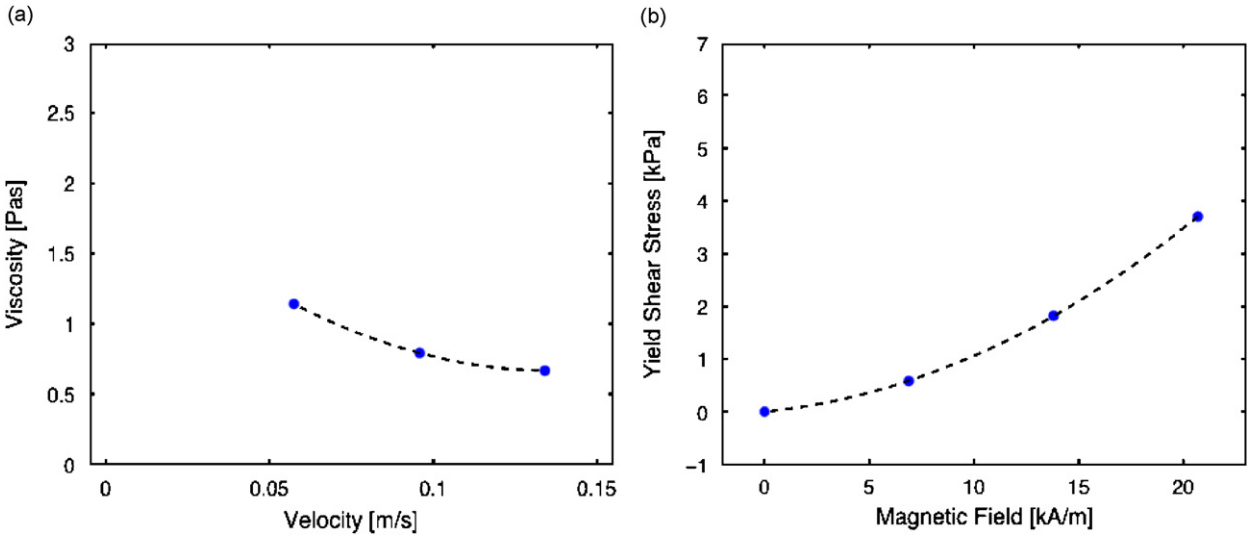

Fig. 10. MR fluid properties used for the analysis: (a) zero-field viscosity and (b) yield shear stress.

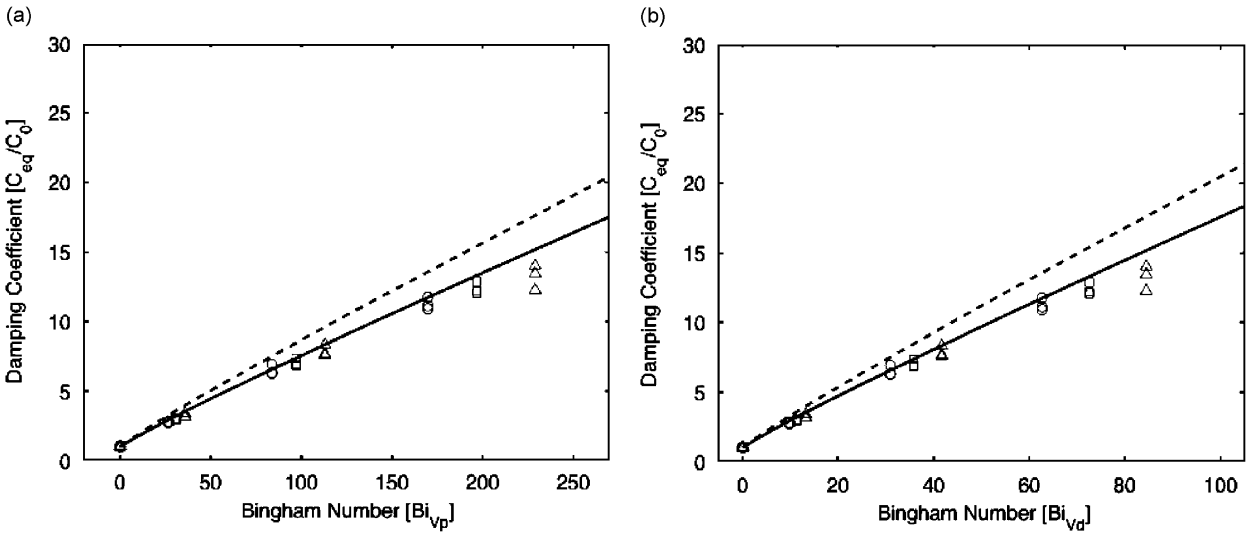

Fig. 11. Experimental and analytical damping coefficients versus Bingham numbers: (a) C_{eq}/C_0 versus Bi_{V_p} and (b) C_{eq}/C_0 versus Bi_{V_d}: (———) mixed mode ($\bar{A} = 2.71$); (- - - - -) flow mode; (Δ) experiment $V_a = 0.03$ m/s; (□) experiment $V_a = 0.05$ m/s; and (○) experiment $V_a = 0.07$ m/s.

4.7. Damping coefficient

Using the experimental data and the analysis model, the damping coefficient, C_{eq}/C_0, is plotted versus the Bingham numbers, Bi_{V_p} and Bi_{V_p}, in Figs. 11(a) and (b). The analysis correlates well with the experiment by using the velocity-dependent viscosity and field-dependent yield shear stress. Therefore, the effectiveness of the nondimensional analysis for the mixed-mode MR damper has been proven. The damping coefficient, C_{eq}/C_0, versus the nondimensional plug thickness, $\bar{\delta}$, obtained by experiment and analysis, is presented in Fig. 12, and correlates well with each other. Fig. 13 shows the damping versus applied current, and the analysis and experimental results agree well. Fig. 14 compares the damping forces obtained by experiment and analysis. Although the damper model could not capture the behavior of the low velocity hysteresis loops and high velocity inertia loops, it could favorably describe the Bingham plastic behavior of the damper force.

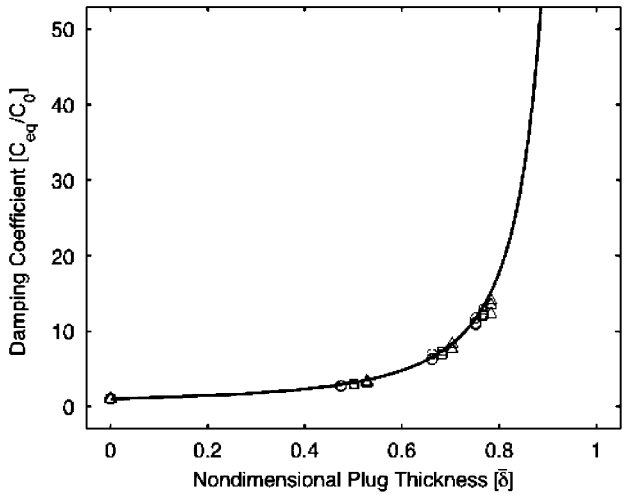

Fig. 12. Experimental and analytical damping coefficients versus nondimensional plug thickness: (———) mixed mode ($\bar{A} = 2.71$) or flow mode; (Δ) experiment $V_a = 0.03$ m/s; (□) experiment $V_a = 0.05$ m/s; and (○) experiment $V_a = 0.07$ m/s.

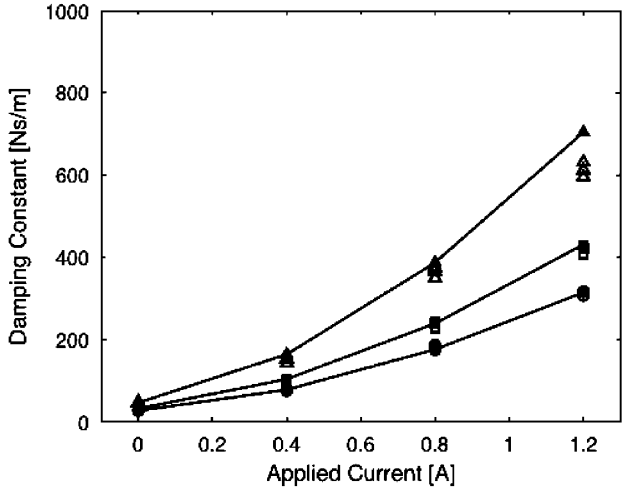

Fig. 13. Experimental and analytical damping constant versus applied current: (—▲—) mixed mode ($\bar{A} = 2.71$), $V_a = 0.03$ m/s; (—■—) mixed mode ($\bar{A} = 2.71$), $V_a = 0.05$ m/s; (—●—) mixed mode ($\bar{A} = 2.71$), $V_a = 0.07$ m/s; (Δ) experiment $V_a = 0.03$ m/s; (□) experiment $V_a = 0.05$ m/s; and (○) experiment $V_a = 0.07$ m/s.

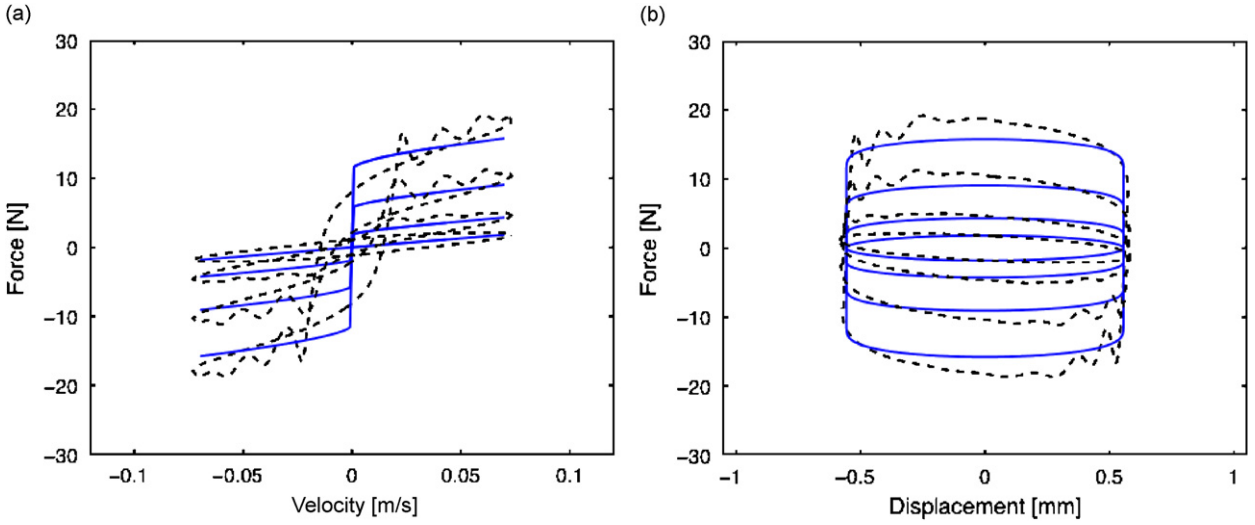

Fig. 14. Measured and analytical forces ($V_a = 0.07$ m/s and $f = 20$ Hz): (a) force versus velocity and (b) force versus displacement: (——) model and (- - - - -) experiment.

5. Conclusion

A mixed-mode MR damper analysis was presented. Based on the nondimensional modeling and analysis approach taken in this study, the following conclusions are made:

(1) On the basis of the Bingham constitutive equation of the MR fluid, a nondimensional model that can favorably describe the mixed-mode operation of the fluid flowing through an annular duct was developed, and the relationships between the nondimensional variables, such as Bingham numbers, the nondimensional plug thickness, the hydraulic amplification ratio, and the equivalent damping coefficient, were investigated analytically.
(2) Bingham numbers were defined by considering piston velocity or average duct velocity through the MR valve. Both Bingham numbers have a role in describing the controllable damping capacity. The Bingham number in terms of the piston velocity was useful when analyzing damper performance with consideration of the external mechanical excitation, and the Bingham number in terms of the average duct velocity was preferred for the analysis focusing on the fluid flow behavior inside the gap. A key conclusion was that the Bingham number was shown to be the independent variable.
(3) The effect of the hydraulic amplification ratio on damping capacity of the damper was also investigated. The nondimensional plug thickness and the damping coefficient can be expressed as a function of either Bingham number and the hydraulic amplification ratio. The analysis of the mixed-mode damper was compared with the flow mode damper case, and the results show that the mixed-mode damper analysis results approach those of the flow mode damper analysis as the hydraulic amplification ratio increases. Therefore, when the hydraulic amplification ratio is small, the mixed-mode damper must be analyzed using the mixed-mode damper analysis.
(4) To validate the nondimensional model of the mixed-mode damper, an MR dashpot damper, featuring a relatively small hydraulic amplification ratio, was designed and fabricated. The damping coefficient, the nondimensional plug thickness, and Bingham numbers were calculated by using the MR fluid properties, the gap geometry, the measured shaft velocity and the damper force. It was observed that the nondimensional analysis correlates well with experiment.

Note that since ER fluids show similar mechanical behaviors (so-called Bingham characteristics) to MR fluids in response to external inputs, the conclusions presented and observed in this study can be

straightforwardly applied to an ER dashpot damper. However, in the process of the implementation of ER and MR dampers, there are differences. For MR dampers, it is necessary to configure electromagnetic coil windings to produce a magnetic field input (proportional to the magnitude of a current over the gap) to activate MR fluids. As a result of the coil windings in MR dampers, there exists both passive duct length and an active duct length, the sum of which equals the total duct length (see Fig. 1). However, for ER dampers, ER fluids are activated by applying an electric field (defined by the magnitude of a voltage across the gap). One-side wall of the gap is connected to the positive (+) voltage input and the other side is connected to the negative (−) voltage input, and then an electric field input occurs across the gap over the entire length of the electrodes in an ER damper. As a result, in ER dampers, the active duct length, L, is the same as the total duct length. Thus, the analyses of this study can be applied to both classes of dampers as long as the correct active length is used.

Acknowledgment

This work was supported by the Post-doctoral Fellowship Program of the Korea Science & Engineering Foundation (KOSEF).

References

[1] R. Stanway, J.L. Sproston, A.K. EI-Wahed, Application of electro-rheological fluids in vibration control: a survey, *Smart Materials and Structures* 5 (4) (1996) 464–482.
[2] J.D. Carlson, D.M. Cantanzarite, K.A. Clair, Commercial magneto-rheological fluid devices, *International Journal of Modern Physics B* 10 (1996) 2857–2865.
[3] S.B. Choi, H.S. Lee, Y.P. Park, H-infinity control performance of a full-vehicle suspension featuring magnetorheological dampers, *Vehicle System Dynamics* 38 (5) (2002) 341–360.
[4] N.D. Sims, R. Stanway, Semi-active vehicle suspension using smart fluid dampers: a modelling and control study, *International Journal of Vehicle Design* 33 (1/2/3) (2003) 76–102.
[5] A.H. Lam, W.H. Liao, Semi-active control of automotive suspension systems with magneto-rheological dampers, *International Journal of Vehicle Design* 33 (1/2/3) (2003) 50–75.
[6] G.M. Kamath, N.M. Wereley, Characterization of magnetorheological helicopter lag dampers, *Journal of American Helicopter Society* 44 (3) (1999) 234–248.
[7] Y.T. Choi, N.M. Wereley, Vibration control of a landing gear system featuring electrorheological/magnetorheological fluids, *Journal of Aircraft* 40 (3) (2003) 432–439.
[8] X. Wang, F. Gordaninejad, Lyapunov-based control of a bridge using magneto-rheological fluid dampers, *Journal of Intelligent Material Systems and Structures* 13 (2002) 415–419.
[9] S.J. Dyke, B.F. Spencer, M.K. Sain, J.D. Carlson, Modeling and control of magnetorheological dampers for seismic response reduction, *Smart Materials and Structures* 5 (1996) 565–575.
[10] K.W. Wang, Y.S. Kim, D.B. Shea, Structural vibration control via electrorheological-fluid-based actuators with adaptive viscous and frictional damping, *Journal of Sound and Vibration* 177 (2) (1994) 227–237.
[11] S.R. Hong, S.B. Choi, M.S. Han, Vibration control of a frame structure using electro-rheological fluid mounts, *International Journal of Mechanical Sciences* 44 (10) (2002) 2027–2045.
[12] H.P. Gavin, R.D. Hanson, F.E. Filisko, Electrorheological dampers, part II: testing and modeling, *ASME Journal of Applied Mechanics* 63 (1996) 676–682.
[13] D.J. Peel, R. Stanway, W.A. Bullough, Dynamic modelling of an ER vibration damper for vehicle suspension applications, *Smart Materials and Structures* 5 (1996) 591–606.
[14] N.M. Wereley, L. Pang, Nondimensional analysis of semi-active electrorheological and magnetorheological dampers using approximate parallel plate models, *Smart Materials and Structures* 7 (1998) 732–743.
[15] J. Lindler, N.M. Wereley, Analysis and testing of electrorheological bypass dampers, *Journal of Intelligent Material Systems and Structures* 10 (1999) 363–376.
[16] S.R. Hong, S.B. Choi, Y.T. Choi, N.M. Wereley, Non-dimensional analysis for effective design of semi-active electrorheological damping control systems, *Proceedings of the Institution of Mechanical Engineers, Part D: Journal of Automobile Engineering* 217 (D12) (2003) 1095–1106.
[17] M.R. Jolly, J.D. Carlson, Controllable squeeze film damping using magnetorheological fluid. *Actuator 96, Fifth International Conferences on New Actuators*, Bremen, Germany, June 1996, pp. 333–336.
[18] N.D. Sims, R. Stanway, A.R. Johnson, P. Mellor, Design, testing, and model validation of an MR squeeze-flow vibration damper, *Damping and Isolation, Proceedings of SPIE* 4331 (2001) 111–120.
[19] G. Yang, B.F. Spencer, J.D. Carlson, M.K. Sain, Large-scale MR fluid dampers: modeling and dynamic performance considerations, *Engineering Structures* 24 (3) (2002) 309–323.

[20] H.P. Gavin, R.D. Hanson, F.E. Filisko, Electrorheological dampers, part I: analysis and design, *ASME Journal of Applied Mechanics* 63 (1996) 669–675.
[21] R.W. Phillips, Engineering Application of Fluids with Variable Yield Stress, PhD Thesis, University of California, Berkeley, 1969.
[22] J.H. Yoo, N.M. Wereley, Design of a high-efficiency magnetorheological valve, *Journal of Intelligent Material Systems and Structures* 13 (10) (2002) 679–687.
[23] H.P. Gavin, Annular Poiseuille flow of electrorheological and magnetorheological materials, *Journal of Rheology* 45 (4) (2001) 983–993.
[24] W. Prager, *Introduction to Mechanics of Continua*, Ginn & Company, New York, 1961, p. 141.
[25] N.M. Wereley, Nondimensional analysis of electrorheological and magnetorheological dampers using a Herschel–Bulkley constitutive model, *Proceedings of the IMECE '03*, San Diego, CA, USA, November 2003, IMECE2003-43310.
[26] N. Rosenfeld, N.M. Wereley, Volume-constrained optimization of magnetorheological and electrorheological valves and dampers, *Smart Materials and Structures* 13 (6) (2004) 1303–1313.
[27] D.Y. Lee, N.M. Wereley, Quasi-steady Herschel–Bulkley analysis of electro- and magneto-rheological flow mode dampers, *Journal of Intelligent Material Systems and Structures* 10 (10) (1999) 761–769.